Available online at www.sciencedirect.com
SCIENCE DIRECT®
International Journal of Solids and Structures 42 (2005) 1759–1776
INTERNATIONAL JOURNAL OF SOLIDS and STRUCTURES
www.elsevier.com/locate/ijsolstr

Structural morphing using two-way shape memory effect of SMA

Maenghyo Cho *, Sanghaun Kim

School of Mechanical and Aerospace Engineering, Seoul National University, San 56-1, Shillim-Dong, Kwanak-Gu, Seoul 151-744, Korea

Received 18 December 2003; received in revised form 14 July 2004
Available online 21 September 2004

Abstract

One-way shape memory effect (SME) is not suitable mechanism for application to the repeated actuation of an shape memory alloy (SMA) wire because the host structure does not return to its initial shape after it cools down. In the present study, the two-way SME under residual stress is considered. A structure using the two-way effect returns to its initial shape by increasing or decreasing temperature under an initially given residual stress. A thermo-mechanical constitutive equation of SMA proposed by Lagoudas et al. was employed in the present study. Laminated composite plate and beam are considered as simple morphing structural components. The modeling of plate and beam are based on first-order shear deformable laminated composite plate theory with large deflection and large deformable beam theory respectively. Numerical results of fully coupled SMA–composite structures are presented. The proposed actuation mechanism based on the two-way SMA effect and a simulation algorithm can be used as a powerful morphing mechanism and simulation tool for structures.

Keywords: SMA; Residual stress; Two-way SME; Structural morphing; Nonlinear behavior

1. Introduction

Shape memory alloys (SMA) wire and patch are often used in smart structures as active components (Birman, 1997). Their capability to provide large recovery forces and displacements has been useful in various engineering applications, including devices for controlling the shapes of spaceship antennas, aircraft wings, and submarine sterns or the vibrations of these structures.

* Corresponding author. Tel.: +82 2 880 1695; fax: +82 2 886 1645/1693.
E-mail address: mhcho@snu.ac.kr (M. Cho).

0020-7683/$ - see front matter © 2004 Elsevier Ltd. All rights reserved.
doi:10.1016/j.ijsolstr.2004.07.010

There are two ways to transform the phase of SMA. One is by changing temperature and the other, by applying stresses. The phase transformation by a temperature change is specified by four different temperatures i.e. martensite finish (M_f), start (M_s), austenite start (A_s) and finish temperatures (A_f). Phase transformation is accomplished at each of start or finish temperature. And these four transformation temperatures strongly depend on the applied residual stress.

Stress induction at a given temperature brings about phase transformation from the austenite phase to the detwinned martensite phase. Here, 'detwinned' means deformed phase that is deformed by stress inducing at austenite or martensite phase. The phase transformation by this process is similar to the deformation process in plasticity. But in phase transformation of SMA, the yield stress strongly depends on the temperature, that is, the yield stress varies as the temperature varies.

Shape memory effect and superelasticity (pseudo-elasticity) of SMA are usually considered in the application of actuators. First, when SMA is initially in the austenite phase at a certain temperature between the austenite finish and martensite start temperatures, stress induction causes the so-called "forward phase transformation", that is, transformation from the austenite phase into the detwinned martensite phase. During this process, we can obtain a large residual strain, whose maximum value reaches up to 9%. After reaching the maximum strain, heating above the austenite finish temperature removes the transformation strain; this removals is called "the reverse transformation". In reverse transformation, large recovery force of SMA can be obtained. In NiTinol, the recovery force is between 500 and 900 MPa. This cyclic process is called as shape memory effect (SME).

Second, when SMA is at a certain temperature above the austenite finish temperature, induced stress transforms the SMA from the austenite phase into the detwinned martensite phase. Unloading the stress allows the SMA to recover its initial shape by transforming from the detwinned martensite into the austenite phase. This loading (forward transformation) and unloading (reverse transformation) process is known as pseudo-elasticity. Most engineering applications using SMA takes advantage of the above mentioned two properties of SMA.

Recent researches on SMA have mainly focused on two items. One is the characterization of the thermo-mechanical behavior of SMA materials (Tanaka et al., 1986; Liang and Rogers, 1990, 1992; Brinson, 1993; Brinson and Lammering, 1993; Abeyaratne et al., 1993; Abeyaratne and Kim, 1997; Lagoudas et al., 1996) and the other is the actuator application of one-way shape memory effect (SME). However, the one-way effect cannot provide suitable mechanism of SMA actuator because the host structure does not return to its initial shape after it is cooled. Therefore, in the present study, we consider the two-way SME under residual stresses. An SMA wire was attached to the midpoint or both edges of a composite panel. This panel returns to its initial shape when the temperature of SMA is increased or decreased in the range of applicable temperature under the initial residual stress.

In the modeling of the thermo-mechanical behavior of SMA, a phenomenological material model (Boyd and Lagoudas, 1996; Lagoudas et al., 1996) based on Gibb's free energy function was employed. The Gibbs free energy (which is stress-based) is chosen herein, instead of the Helmholtz free energy (which is strain-based), to facilitate the comparison between model prediction and experimental result, which are often performed using stress control. Evolution equations for internal variables represent the dissipative material behavior. Thermo-mechanical consistency was ensured because the constitutive model satisfied the Clausius–Duhem inequality (Truesdell and Noll, 1965). Also, to solve the SMA constitutive equation, we used the Cutting Plane Return Mapping Algorithm (Qidwai and Lagoudas, 2000; Simo and Hughes, 1998; Lubliner, 1990). These are described in Section 2. In Section 3, laminated composite plates and beam are considered as simple morphing structural components. The modeling of these components was based on the first-order shear deformable laminated composite plates with von Karman nonlinearity and the large deformable beam respectively. Solution algorithm for the geometric nonlinear problem (Newton–Raphson Method) is described (Zienkiewicz and Taylor, 2000).

The numerical analysis algorithm for SMA–composite coupled structures is presented in Section 4. This algorithm integrates the analytical solution for SMA and FEM solution for host structures.

Numerical solutions in Section 5 reveal the various deformable behavior of the assembly structure of SMA wire and composite panel in the applied temperature range. The results of numerical simulation of the panel-morphing based on the two-way effect of SMA under residual stress are presented.

2. SMA constitutive model

2.1. Thermo-mechanical constitutive equation for SMA

Shape memory alloy (SMA) can transform itself by moving into austenite or martensite phase. To present the phase transformation, the total Gibb's free energy of SMA is expressed as a function of stress, temperature, and mixing region Gibb's free energy. Stresses and temperatures are main factors in the phase transformation.

$$G(\sigma_{ij},T)=G^{\mathrm{A}}(\sigma_{ij},T)+\xi\left[G^{\mathrm{M}}(\sigma_{ij},T)-G^{\mathrm{A}}(\sigma_{ij},T)\right]+G^{\mathrm{mix}} \tag{1}$$

where G^{mix} is the Gibb's free energy in the mixing region which depends on the inelastic strain during transformation. This equation is similar to the plastic hardening function to describe plastic deformation.

Gibb's free energy in the mixing region is a function of stress, temperature, martensite volume fraction, and transformation strain. Transformation strain is generated by the small change of stress and temperature. Thus, the Gibb's free energy in the mixing region can be assumed as a function of only the martensite volume fraction (ξ) and transformation strain ($\varepsilon^{\mathrm{t}}_{ij}$).

$$G^{\mathrm{mix}}=G^{\mathrm{mix}}\left(\sigma_{ij},T,\xi,\varepsilon^{\mathrm{t}}_{ij}\right)=f\left(\xi,\varepsilon^{\mathrm{t}}_{ij}\right) \tag{2}$$

From Eqs. (1) and (2), the total Gibb's free energy of SMA is rewrote as below:

$$G^{\alpha}(\sigma_{ij},T)=-\frac{1}{\rho}\frac{1}{2}S^{\alpha}_{ijkl}\sigma_{ij}\sigma_{kl}-\frac{1}{\rho}\alpha^{\alpha}_{ij}\sigma_{ij}\Delta T+c^{\alpha}\left[\Delta T-T\ln\left(\frac{T}{T_0}\right)\right]-s^{\alpha}_0T+u^{\alpha}_0,\quad \alpha=\mathrm{A}\text{ or }\mathrm{M} \tag{3}$$

$$G(\sigma_{ij},T,\xi,\varepsilon^{\mathrm{t}}_{ij})=G^{\mathrm{A}}(\sigma_{ij},T)+\xi\left[G^{\mathrm{M}}(\sigma_{ij},T)-G^{\mathrm{A}}(\sigma_{ij},T)\right]+f(\xi,\varepsilon^{\mathrm{t}}_{ij}) \tag{4}$$

Eq. (3) describes the uni-phase Gibb's free energy. In order to express martensite Gibb's free energy ($\alpha=\mathrm{M}$) or austenite Gibbs free energy ($\alpha=\mathrm{A}$), respectively, uni-phase Gibbs free energy is used for a unified expression. It consists of two internal variables, that is, stress and temperature and it can be obtained from Gibb's free energy and the 1st law of thermodynamics. Using this uni-phase constitutive equation and martensite volume fraction, Eq. (4) describes the total Gibb's free energy, which expresses the relation between two different phases. Here, using the hardening (transformation) function $f(\xi,\varepsilon^{\mathrm{t}}_{ij})$ similar to the hardening function in plasticity theory, the transformation function expresses energy dissipation and energy conservation. Eq. (4) cannot describe the reorientation effect in the microscopic point of view. But this equation adequately describes the macroscopic phenomenological behaviors of SMA.

$$G(\sigma_{ij},T,\xi,\varepsilon^{\mathrm{t}}_{ij}):=-\frac{1}{\rho}\frac{1}{2}\sigma:\overline{S}:\sigma-\frac{1}{\rho}\sigma:[\bar{\alpha}(T-T_0)]+\bar{c}\left[(T-T_0)-T\ln\left(\frac{T}{T_0}\right)\right]-\bar{s}_0T+\bar{u}_0+f(\xi) \tag{5}$$

$$\begin{bmatrix}\overline{S}:=S^{\mathrm{A}}+\xi\Delta S\\ \bar{\alpha}:=\alpha^{\mathrm{A}}+\xi\Delta\alpha\\ \bar{c}:=c^{\mathrm{A}}+\xi\Delta c\\ \bar{s}_0:=s^{\mathrm{A}}_0+\xi\Delta s_0\\ \bar{u}_0:=u^{\mathrm{A}}_0+\xi\Delta u_0\end{bmatrix}\qquad\begin{bmatrix}\Delta S=S^{\mathrm{M}}-S^{\mathrm{A}}\\ \Delta\alpha=\alpha^{\mathrm{M}}-\alpha^{\mathrm{A}}\\ \Delta c=c^{\mathrm{M}}-c^{\mathrm{A}}\\ \Delta s_0=s^{\mathrm{M}}_0-s^{\mathrm{A}}_0\\ \Delta u_0=u^{\mathrm{M}}_0-u^{\mathrm{A}}_0\end{bmatrix} \tag{6}$$

where S is the compliance, α is the thermal expansion, c is the specific heat, s_0 is an initial entropy and u_0 is the initial internal energy. Eqs. (5) and (6) are obtained by changing Eq. (4) with properties of two phases, that is, austenite and martensite phase of SMA.

SMA behaves hysteretically by stress inducing or temperature increasing, i.e. SMA transforms austenite or martensite into detwinned martensite phase by stress inducing, and martensite into austenite phase by temperature increasing. Such constraint conditions of SMA behavior are given by the thermodynamic approach, that is, Clausius–Duhem inequality (Trusdell and Noll strong local form) in conjunction with the second law of thermodynamics (Ortin and Planes, 1989; Raniecki and Lexcellent, 1994; Sun and Hwang, 1993a,b; Boyd and Lagoudas, 1996). The following equation expresses the energy dissipation using the 2nd law of thermodynamics, i.e. Trusdell and Noll strong local form except for heat generation and radiation ($T\dot{\eta} \geqslant 0$).

$$T\dot{\eta} = \sigma_{ij}\dot{\varepsilon}_{ij} - \rho\dot{\psi} - \rho s\dot{T} \geqslant 0 \tag{7}$$

Since the total Gibb's free energy has four internal variables which are σ_{ij}, T, ξ, ε^{t}_{ij}, the rate of total Gibb's free energy $\dot{G}$ can be written as

$$\dot{G} = \frac{\partial G}{\partial \sigma_{ij}}\dot{\sigma}_{ij} + \frac{\partial G}{\partial T}\dot{T} + \frac{\partial G}{\partial \xi}\dot{\xi} + \frac{\partial G}{\partial \varepsilon^{t}_{ij}}\dot{\varepsilon}^{t}_{ij} \tag{8}$$

$$\varepsilon_{ij} = \varepsilon^{te}_{ij} + \varepsilon^{t}_{ij} \tag{9}$$

Using the rate form of the total Gibb's free energy given in Eq. (8) and the total strain, which is decomposed into the thermoelastic strain region and transformation strain region as given in Eq. (9), we can obtain the following local dissipation rate:

$$T\dot{\eta} = \left(\sigma_{ij} - \rho\frac{\partial f}{\partial \varepsilon^{t}_{ij}}\right)\dot{\varepsilon}^{t}_{ij} - \rho\frac{\partial G}{\partial \xi}\dot{\xi} \geqslant 0, \qquad T\dot{\eta} = \phi^{t} \geqslant 0 \tag{10}$$

Here, $\phi^{t} \geqslant 0$ is a consistency condition, which describes energy dissipation. The hardening function $f(\xi, \varepsilon^{t}_{ij})$ is independent of the transformation strain and is always positive. In the present study, only isotropic transformation hardening is considered, and the kinematic transformation hardening is neglected. Because the micro-structure of SMA is changed during transformation, the hardening function must have a return point. These conditions were mentioned in Lagoudas et al. (1996). Based upon the above mentioned conditions, the transformation strain is expressed by the rate of the martensite volume fraction (ξ), which indicates the extent of the transformation. From the above assumptions, we can use the following equations:

$$f = f(\xi), \quad f(0) = 0, \quad f(\xi) \geqslant 0 \tag{11}$$

$$\dot{\varepsilon}^{t}_{ij} = \Lambda_{ij}\dot{\xi} \tag{12}$$

Here, Λ_{ij} is a transformation tensor, which indicates the amount of transformation that occurred. The transformation tensor Λ_{ij} depends on the material constituents of SMA and the direction of axis. Inserting Eqs. (11) and (12) into Eq. (10), the simple form of the energy dissipation equation is obtained as follows:

$$T\dot{\eta} = \left(\sigma_{ij}\Lambda_{ij} - \rho\frac{\partial G}{\partial \xi}\right)\dot{\xi} = \Pi\dot{\xi} \geqslant Y, \qquad T\dot{\eta} = \phi^{t} \tag{13}$$

Here, Π is a thermodynamic force which was named from the concept that thermoelastic or transformation behavior of SMA is generated by a mechanical force associated with the dissipative condition that occurs. The condition $\phi^{t} \geqslant Y$ is consistency condition and consistency equation ($\phi^{t} = \Pi\dot{\xi}$) is expressed by multiplying the thermodynamic force by the martensite volume fraction. Eq. (13) indicates that the energy is

dissipated when ϕ^t exceeds Y. Y is a quantity similar to the yield stress in plasticity. This consistency condition plays an important role in dividing regions into an elastic one and transformation one at a given temperature by applying Kuhn–Tucker condition, mentioned below:

$$\dot{\xi} = \lambda \frac{\partial \phi^t}{\partial \Pi} \tag{14}$$

$$\lambda \geqslant 0 \quad \text{and} \quad \phi^t \leqslant \pm Y \Rightarrow \lambda(\phi^t - (\pm Y)) = 0 \tag{15}$$

$$\begin{aligned} &\Pi < \pm Y^*, \quad \dot{\xi} = 0 : \text{Thermoelastic Region} \\ &\Pi = \pm Y^*, \quad \dot{\xi} > 0 : \text{Transformation Region} \end{aligned} \tag{16}$$

Eq. (14) expresses the associative flow rule. The rate form of martensite volume fraction is associated with the thermodynamic force (Π) and transformation strain is generated in the normal direction of the yield or loading surface. Eq. (15) is a general form of the Kuhn–Tucker condition. Kuhn–Tucker condition is unified condition to describe two or more constraint conditions. It is used to satisfy one of the several constraint conditions of SMA constitutive equation in numerical analysis. If we apply these conditions given in Eqs. (13)–(15) to the SMA constitutive equation, we can obtain the Kuhn–Tucker condition of the SMA constitutive equations given in Eq. (16). Here, Y^* is the replaced value which is related to the thermodynamic force similar to the relationship between consistency equation (ϕ^t) and yield stress (Y). The positive sign is used for the forward transformation (cooling) and the negative sign is used for reverse transformation (heating) process respectively, because SMA behaves hysteretically in the loading–unloading and heating–cooling process. Since it is assumed that the SMA deformation is rate-independent, the consistency equation ϕ^t is rate-independent.

$$\dot{\phi}^t = 0 \tag{17}$$

Eq. (17) expresses a tangent-consistency condition during transformation. By means of consistency-thermodynamic force relationship given in Eq. (13) and the assumption that the dissipation potential has a quadratic form, the tangent-consistency condition about thermodynamic force is derived as follows:

$$\dot{\Pi} = 0 \tag{18}$$

Eq. (18) also expresses a tangent-consistency condition during phase transformation. From Eq. (18), we can obtain the tangent form given as

$$-\left(\frac{\partial \Pi}{\partial \xi} + \frac{\partial \Pi}{\partial \varepsilon_{ij}^t} \Lambda_{ij}\right) \dot{\xi} = \frac{\partial \Pi}{\partial \sigma_{ij}} \dot{\sigma}_{ij} + \frac{\partial \Pi}{\partial T} \dot{T} \tag{19}$$

$$\begin{aligned} \Pi &= \sigma_{ij} \Lambda_{ij} - \rho \frac{\partial G}{\partial \xi} \\ &= \sigma : \Lambda + \frac{1}{2} \sigma : \Delta S : \sigma + \sigma : \Delta\alpha (T - T_0) - \rho \Delta c \left[(T - T_0) - T \ln \left(\frac{T}{T_0} \right) \right] \\ &\quad + \rho \Delta s_0 T - \rho \Delta u_0 - \rho \frac{\partial f}{\partial \xi} \end{aligned} \tag{20}$$

The rate forms of stress, strain, temperature and martensite volume fraction in the transformation region are derived from Eqs. (19) and (20).

2.2. Numerical algorithms of SMA constitutive model

For the numerical solution of SMA constitutive equation, we use the Convex Cutting Plane Return Mapping Algorithm presented by Simo and Hughes (1998). The advantage of the given algorithm lies in its simplicity and bypassing the need for computing the gradients (less time cost in calculation), because if one adds another internal state variable in the model, more gradient quantities must be accounted for. Evaluating such gradients may prove difficult and computationally expensive. Through the comparison with closest point return mapping algorithm, the superiority and advantage of convex cutting plane return mapping algorithm are explained minutely in the reference (Qidwai and Lagoudas, 2000). Though closest point projection return mapping algorithm uses the tangent form, Eq. (19), convex cutting plane return mapping algorithm uses the discrete form of thermodynamic force, Eq. (31) which is more simple and easier to calculate than Eq. (19).

The rate form of the thermoelastic, transformation and total strains are derived as follows:

$$\dot{\varepsilon}^{\mathrm{t}}_{ij} = \Lambda_{ij}\dot{\xi} \tag{21}$$

$$\varepsilon^{\mathrm{te}}_{ij} = -\rho\frac{\partial G}{\partial \sigma_{ij}} = \overline{S} : \sigma + \bar{\alpha}(T - T_0) \tag{22}$$

$$\varepsilon_{ij} = \overline{S} : \sigma + \bar{\alpha}(T - T_0) + \varepsilon^{\mathrm{t}}_{ij} \tag{23}$$

On the other hand, because the total strain is a function of stress, temperature, and martensite volume fraction, we can obtain the following equation:

$$\begin{aligned} \mathrm{d}\varepsilon &= \frac{\partial \varepsilon}{\partial \sigma}\mathrm{d}\sigma + \frac{\partial \varepsilon}{\partial T}\mathrm{d}T \pm \frac{\partial \varepsilon}{\partial \xi}\mathrm{d}\xi = \overline{S}\,\mathrm{d}\sigma + \bar{\alpha}\,\mathrm{d}T \pm \frac{\partial \varepsilon}{\partial \xi}\mathrm{d}\xi \\ &= \overline{S}\,\mathrm{d}\sigma + \bar{\alpha}\,\mathrm{d}T \pm [\Delta S : \sigma + \Delta\alpha(T - T_0) + \Lambda]\mathrm{d}\xi \end{aligned} \tag{24}$$

Here, the positive sign indicates the forward phase transformation and the negative sign indicates the reverse phase transformation. Because the convex cutting plane return mapping algorithm is the forward Euler method ($\beta = 0$), the rate form of the transformation strain at t_{n+1} can be expressed in the following forms:

$$\dot{\varepsilon}^{\mathrm{t}}_{ij} = \Lambda_{ij}\dot{\xi} \Rightarrow \varepsilon^{\mathrm{t}}_{n+1} = \varepsilon^{\mathrm{t}}_{n} + (\xi_{n+1} - \xi_n)\Lambda_n \Rightarrow \Delta\varepsilon^{\mathrm{t}}_{n+1} = \Delta\xi_{n+1}\Lambda_n \tag{25}$$

By applying Eq. (25) to Eq. (24) and noting that ε and T are fixed during the return mapping (transformation correction) stage, we can express the transformation strain increment at an isothermal process.

$$\Delta\varepsilon^{\mathrm{t}}_{n+1} = -\overline{S}_{n+1} : \Delta\sigma_{n+1} \mp [\Delta S : \sigma_{n+1} + \Delta\alpha(T_{n+1} - T_0)]\Delta\xi_{n+1} \tag{26}$$

$$\begin{bmatrix} \overline{S}_{n+1} := S^{\mathrm{A}} + \xi_{n+1}(S^{\mathrm{M}} - S^{\mathrm{A}}) \\ \bar{\alpha}_{n+1} := \alpha^{\mathrm{A}} + \xi_{n+1}(\alpha^{\mathrm{M}} - \alpha^{\mathrm{A}}) \end{bmatrix} \tag{27}$$

(1) *Thermoelastic prediction ($\Pi < \pm Y^*$)*

Because the deformation behavior of SMA is within the elastic region, S_n^{-1} and $\bar{\alpha}_n$ have certain values and $\varepsilon^{\mathrm{t}}_n$ and ξ_n are fixed to zero.

$$\sigma^{(0)}_{n+1} = \overline{S}_n^{-1} : \left[\varepsilon_{n+1} - \bar{\alpha}_n(T_{n+1} - T_0) - \varepsilon^{\mathrm{t}}_n\right] \tag{28}$$

$$\Pi^{(0)}_{n+1} := \Pi\left(\sigma^{(0)}_{n+1}, T_{n+1}, \xi_n\right) \leqslant \pm Y^* \tag{29}$$

(2) *Transformation correction* ($\Pi > \pm Y^* \rightarrow \Pi = \pm Y^*$)

In the region of transformation, thermodynamic force is greater than $\pm$Y*. This deviated value causes the transformation strain. To prevent this undesirable transformation strain, the deviated thermodynamic force is modified to have $\pm$Y*. By Eqs. (25) and (26), the increment of stress during transformation is expressed in the following form:

$$\Delta\sigma_{n+1} = -\overline{S}_{n+1}^{-1} : [\pm(\Delta S : \sigma_{n+1} + \Delta\alpha(T_{n+1} - T_0) + \Lambda_n)]\Delta\xi_{n+1} \tag{30}$$

- *Residual thermodynamic force*

Thermodynamic force is a function of stress and martensite volume fraction as shown in Eq. (20), i.e. $\Pi_{n+1} := \Pi(\sigma_{n+1}, \xi_{n+1})$. After discretizing the thermodynamic force, following equation is derived:

$$\Pi_{n+1} + \frac{\partial \Pi_{n+1}}{\partial \sigma} : \Delta\sigma_{n+1} + \frac{\partial \Pi_{n+1}}{\partial \xi}\Delta\xi_{n+1} = \pm Y^* \tag{31}$$

Inserting Eq. (30) into Eq. (31), the rate form of martensite volume fraction is derived.

$$\Delta\xi_{n+1} = \frac{\Pi_{n+1} - (\pm Y)}{\pm\frac{\partial \Pi_{n+1}}{\partial \sigma} : \overline{S}_{n+1}^{-1} : [\Delta S : \sigma_{n+1} + \Delta\alpha(T_{n+1} - T_0) + \Lambda_n] - \frac{\partial \Pi_{n+1}}{\partial \xi}} \tag{32}$$

(3) *Geometrical interpretation*

Using the rate form of martensite volume fraction derived in Eq. (32), all the internal variables at t_{n+1} of SMA constitutive equation are obtained by adding the incremental quantities the values given at t_n as below:

$$\begin{aligned} \xi_{n+1} &= \xi_n + \Delta\xi_{n+1} \\ \varepsilon_{n+1}^{t} &= \varepsilon_n^{t} + \Delta\varepsilon_{n+1}^{t} \\ \sigma_{n+1} &= \sigma_n + \Delta\sigma_{n+1} \end{aligned} \tag{33}$$

3. Host structure analysis

Because the transformation strain of SMA is over 5%, the deformation of the structure using the SMA effect becomes larger. Thus, we should consider the geometric nonlinearity in the host structure to accurately predict the behaviors of the host structure and SMA wire combined.

In the present study, we consider the first order shear deformable plate theory with a large deflection (von Karman plate theory) and large deformable beam theory with Green–Lagrangian strain in composite structures. The schematics of plate and beam for finite-element mesh are shown in Fig. 1. Here, four-node element is used for plate model and nine-node plane element is used for beam model, respectively.

3.1. First-order shear deformable plate theory with large deflection

The displacement assumption for a first order shear deformation plate is given as

$$u_\alpha = u_\alpha^0 - z\theta_\alpha, \quad u_3 = w(X_1, X_2), \qquad \alpha = 1, 2 \tag{34}$$

where u_α^0 is the mid-plane in-plane displacement and θ_α is the rotational displacement. u_1, u_2, w are translational displacements in (X_1, X_2, X_3) directions, respectively. X_1, X_2 are in-plane coordinates in the undeformed configuration.

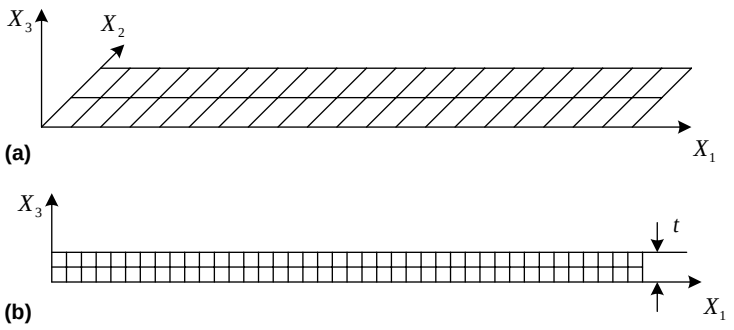

Fig. 1. The schematics of (a) plate and (b) beam for finite-element mesh.

The strain–displacement relationship of each part is express as below:

(1) *Membrane part*

$$\varepsilon_{\alpha\beta} = \frac{1}{2}\left(\frac{\partial u_\alpha^0}{\partial X_\beta} + \frac{\partial u_\beta^0}{\partial X_\alpha} + \frac{\partial w}{\partial X_\alpha}\frac{\partial w}{\partial X_\beta}\right), \quad \alpha,\beta = 1,2 \tag{35}$$

(2) *Bending part*

$$\varepsilon_{\alpha\beta} = -\frac{1}{2}\left(\frac{\partial \theta_\alpha}{\partial X_\beta} + \frac{\partial \theta_\beta}{\partial X_\alpha}\right)z, \quad \alpha,\beta = 1,2 \tag{36}$$

(3) *Transverse shear part*

$$\gamma_{\alpha 3} = -\theta_\alpha + \frac{\partial w}{\partial X_\alpha}, \quad \alpha = 1,2 \tag{37}$$

3.2. The large deformable beam theory

The nonlinear geometric relationship between strain and displacement field is given as follows for beam theory

$$\varepsilon_{\alpha\beta} = \frac{1}{2}\left(\frac{\partial u_\alpha}{\partial X_\beta} + \frac{\partial u_\beta}{\partial X_\alpha} + \frac{\partial u_\gamma}{\partial X_\alpha}\frac{\partial u_\gamma}{\partial X_\beta}\right), \quad \alpha,\beta,\gamma = 1,2 \tag{38}$$

3.3. The numerical algorithm of geometric nonlinear problem

Newton–Raphson method is used for FEM analysis on the behavior of the host structure from geometric nonlinear plate and beam theories. Here, total Lagrangian description is used and the four-nine-node quadrilateral elements are used. The tolerance is chosen to 1.0×10^{-6} for the convergence criteria of the algorithm.

$$\underset{\sim}{\varepsilon} = \underset{\sim}{B}(\vec{a})\vec{u} \tag{39}$$

$$\underset{\sim}{S} = \underset{\sim}{C}\ \underset{\sim}{\varepsilon} = \underset{\sim}{C}\ \underset{\sim}{B}(\vec{a})\vec{u} \tag{40}$$

$$\begin{cases} \vec{a} = [w_I], \quad \vec{u} = [u_I, v_I, w_I, \theta_{xI}, \theta_{yI}] & : \text{ for von Karman plate theory} \\ \vec{a} = \vec{u} = [u_I, v_I] & : \text{ for large deformable beam theory} \end{cases} \tag{41}$$

$$\frac{\partial \underset{\sim}{\varepsilon}}{\partial \vec{u}} = \underset{\sim}{B}(\vec{a}), \qquad \frac{\partial \underset{\sim}{S}}{\partial \vec{u}} = \underset{\sim}{C}\,\underset{\sim}{B}(\vec{a}) \tag{42}$$

Eq. (39) is the unified expression of strain–displacement relation in both von Karman plate theory (Eqs. (35)–(37)) and large deformable beam theory (Eq. (38)). Eq. (40) shows a unified stress–strain (displacement) relation. Eq. (41) describes $\vec{a}$ and $\vec{u}$ in the above mentioned equations. Eq. (42) indicates the derivation of the stress and strain about the displacement.

Using Eq. (42), the internal force vector and the linearization equation are given as below:

(1) *Internal force*

$$\vec{f}^{\text{int}} = \int_{\Omega_0} \underset{\sim}{B}^{\mathrm{T}}(\vec{a})\,\underset{\sim}{S}\,\mathrm{d}\Omega_0 \tag{43}$$

(2) *Linearization*

$$\left\{ \int_{\Omega_0} \underset{\sim}{B}^{\mathrm{T}}(\vec{a})\,\underset{\sim}{C}\,\underset{\sim}{B}(\vec{a})\,\mathrm{d}\Omega_0 + \int_{\Omega_0} \frac{\partial \underset{\sim}{B}^{\mathrm{T}}(\vec{a})}{\partial \vec{u}}\,\underset{\sim}{S}\,\mathrm{d}\Omega_0 \right\} \dot{\vec{u}} = \dot{\vec{f}}^{\text{ext}} \tag{44}$$

Here, $\vec{u}$ is the nodal displacement vector, $\vec{a}$ is the displacement vector associated with geometric nonlinearity, I is the node number, $\underset{\sim}{\varepsilon}$ is the Green–Lagrange strain matrix, $\underset{\sim}{S}$ is the second kind Piolar–Kirchoff stress matrix and $\underset{\sim}{C}$ is the stiffness matrix.

3.4. The stiffness matrix of host structure

$$\underset{\sim}{Q} = \frac{1}{1 - v_{12}v_{21}} \begin{bmatrix} E_1 & v_{21}E_1 & 0 \\ v_{12}E_2 & E_2 & 0 \\ 0 & 0 & G_{12}(1 - v_{12}v_{21}) \end{bmatrix}, \quad v_{12}E_2 = v_{21}E_1 \tag{45}$$

$\underset{\sim}{Q}$ is the stiffness matrix under the in-plane stress assumption when the fiber direction is aligned to the direction 1. Here, E_1 is the Young's modulus of the fiber direction, E_2 is the Young's modulus of the orthogonal direction of the fiber and v_{12}, v_{21} are the Poisson's ratio.

$$\begin{cases} \overline{Q}_{11} = Q_{11} \cdot \cos^4\theta + Q_{22} \cdot \sin^4\theta + Q_{12} \cdot 2\cos^2\theta \cdot \sin^2\theta + Q_{66} \cdot 4\cos^2\theta \cdot \sin^2\theta \\ \overline{Q}_{12} = (Q_{11} + Q_{22} - 4Q_{66}) \cdot \cos^2\theta \cdot \sin^2\theta + Q_{12}(\cos^4\theta + \sin^4\theta) \\ \overline{Q}_{22} = Q_{11} \cdot \sin^4\theta + 2(Q_{12} + 2Q_{66}) \cdot \cos^2\theta \cdot \sin^2\theta + Q_{22} \cdot \cos^4\theta \\ \overline{Q}_{16} = (Q_{11} - Q_{12} - 2Q_{66}) \cdot \cos^3\theta \cdot \sin\theta + (Q_{12} - Q_{22} + 2Q_{66}) \cdot \cos\theta \cdot \sin^3\theta \\ \overline{Q}_{26} = (Q_{11} - Q_{12} - 2Q_{66}) \cdot \cos\theta \cdot \sin^3\theta + (Q_{12} - Q_{22} + 2Q_{66}) \cdot \cos^3\theta \cdot \sin\theta \\ \overline{Q}_{66} = (Q_{11} + Q_{22} - 2Q_{12} - 2Q_{66}) \cdot \cos^2\theta \cdot \sin^2\theta + Q_{66}(\cos^4\theta + \sin^4\theta) \end{cases} \tag{46}$$

Eq. (46) expresses the each layer stiffness component when the fiber direction is aligned with the angle θ with the x-axis.

$$\underset{\sim}{C} = \sum_{k=1}^{n} \overline{\underset{\sim}{Q}}^{k} (z_k - z_{k-1}) \tag{47}$$

Here, $\underset{\sim}{C}$ is the stiffness matrix of the overall layer, $\overline{\underset{\sim}{Q}}^{k}$ is the stiffness matrix of the kth layer with a certain fiber angle direction. z_k and z_{k-1} are the top and bottom position coordinate value in the thickness direction of the kth layer. From the summation of each layer, the stiffness matrix of host structure is calculated.

4. Numerical algorithm for SMA–composite structure

First, the length of an SMA wire and the deformation of a composite structure are calculated by the constitutive equation derived in Sections 2 and 3 at a specified temperature and stress. Next, the length of the SMA wire is calculated at a new temperature and initial stress. If there is a difference in the deformation between the SMA wire and the host structure, updated stress (or force) is applied to both the SMA wire and the composite structure. The two lengths are compared until the difference of the two length converges within a specified error range (in the present study, this range was chosen to be 10^{-5}). At this time, the converged stress is the proper equilibrium stress for the given temperature, that is, the actuator device should be in static equilibrium at a certain temperature and stress (force) condition. This algorithm is described in the flow chart shown in Fig. 2.

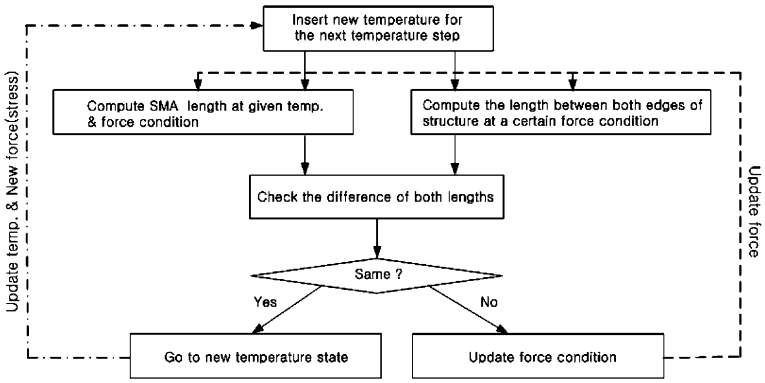

Fig. 2. Numerical procedure for simulation of the behavior of SMA–composite structure.

Table 1
SMA and composite material properties

SMA property $\varphi = 0.30$ mm (SMA diameter)		Composite material property (Graphite–epoxy Layer)
$E^{A} = 30.0 \times 10^{3}$ MPa	$E^{M} = 13.0 \times 10^{3}$ Mpa	Geometry: 200 mm × 10 mm (case 1)
$\nu^{A} = \nu^{M} = 0.33$		: 200 mm × 5 (7) mm (case 2)
$\alpha^{A} = 11.0 \times 10^{-6}$/°C	$\alpha^{M} = 6.6 \times 10^{-6}$/°C	Thickness = 0.125 mm
$H = 0.050$	$I = 0.00$	$E_{0^\circ} = 144.23 \times 10^{3}$ N/mm^2
$A_{0s} = 301$ K (=28 °C)	$A_{0f} = 316$ K (=43 °C)	$E_{90^\circ} = 9.66 \times 10^{3}$ N/mm^2
$M_{0s} = 273$ K (=0 °C)	$M_{0f} = 260$ K (=−13 °C)	$G = 4.14 \times 10^{3}$ N/mm^2

The superscript "A" indicates Austenite phase and the superscript "M" indicates Martensite phase.
The subscript "s" indicates "start", the subscript "f" indicates "finish" and The subscript "0" indicates "stress free".

5. Numerical results and discussions

Material properties of SMA and composite material (G/E_p) for structural analysis are given in Table 1. We consider the fully trained SMA wire with 5% transformation strain. The SMA in the present study is actuated by the one-way behavior by stress and also by the two-way behavior by temperature,

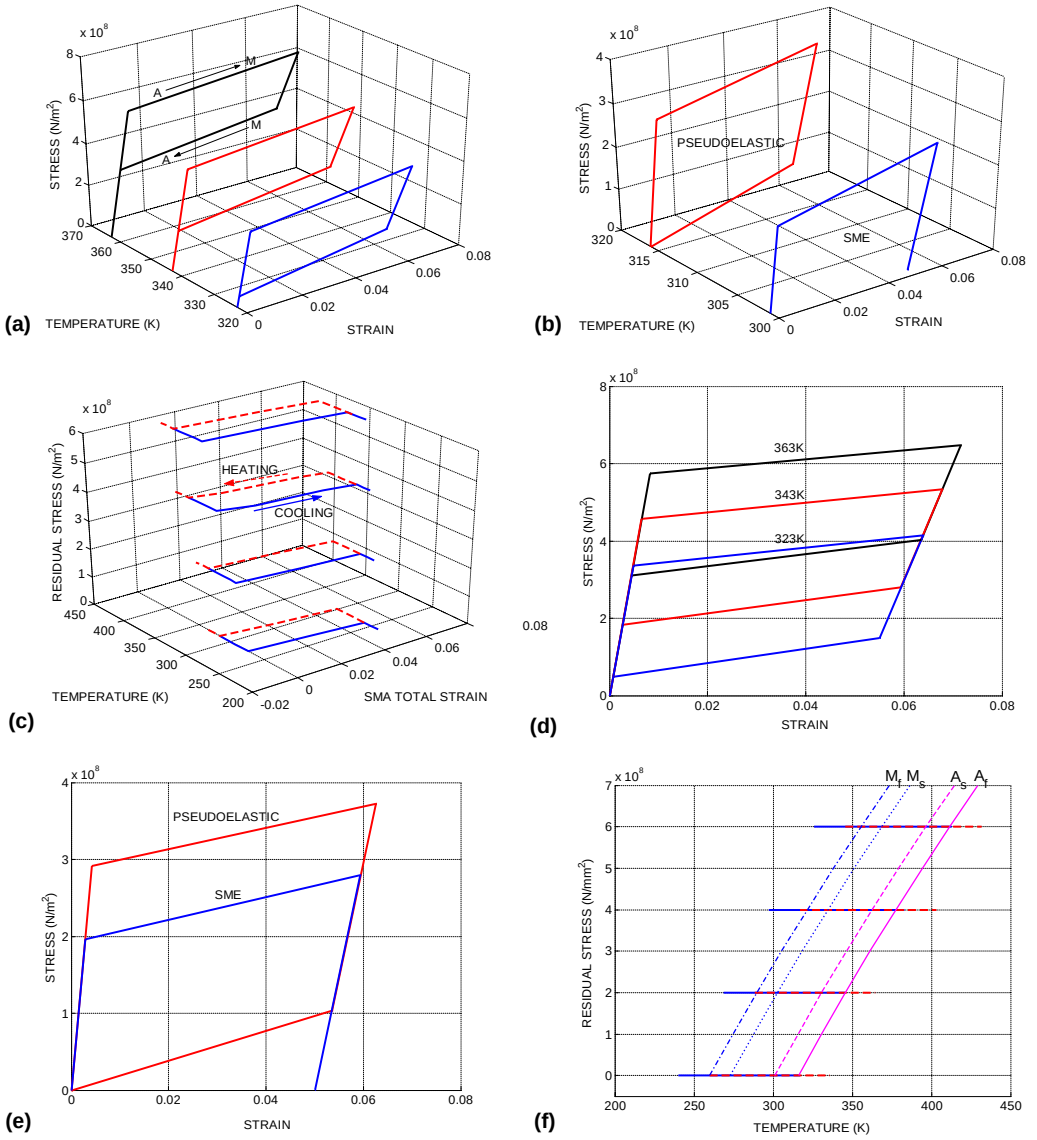

Fig. 3. (a) Simulation results of stress–temperature–strain SMA behavior in pseudo-elasticity, (b) simulation results of stress–temperature–strain SMA behavior in pseudo-elasticity and shape memory effect (SME), (c) simulation results of two-way shape memory effect at each residual stresses (0, 200, 400, 600 Mpa), (d) simulation results of stress–temperature SMA behavior in pseudo-elasticity, (e) simulation results of stress–temperature SMA behavior in pseudo-elasticity and shape memory effect (SME), (f) simulation results of residual stress–temperature curve (two-way shape memory effect) at each residual stresses (0, 200, 400, 600 Mpa) with the four transformation temperature curves.

simultaneously. It is reported that the two-way transformation strain of Cu (copper)–Zn (zinc)–Al (aluminum) SMA is 2%, but the two-way transformation strain of Ni–Ti SMA is 5% in many papers (Araujo et al., 1999; Bo and Lagoudas, 1999; šak et al., 2003). In these reasons, we chose the 5% for the two-way transformation strain.

5.1. Numerical simulation of SMA constitutive equation

Fig. 3(a)–(f) show the results of the numerical simulations of the pseudo-elastic behavior of SMA above the austenite finish temperature (Fig. 3(a) and (d)), the behavior of the shape memory effect between the austenite finish and martensite start temperature (Fig. 3(b) and (e)) and the behavior of the two-way shape memory effect on the each residual stress (Fig. 3(c) and (f)). In Fig. 3(f), the four transformation temperature curves along the residual stresses are indicated. The residual stress-transformation temperature equation is derived as follows (Lagoudas et al., 1996):

$$\frac{\mathrm{d}T}{\mathrm{d}\sigma} = -\frac{H + \Delta S\sigma + \Delta\alpha\Delta T}{\rho\Delta s_0 + \Delta\alpha\sigma} \tag{48}$$

In the four transformation temperature curves along the residual stress (Fig. 3(f)), the start and finish of phase transformation is accomplished at each transformation start and finish temperature in heating–cooling process.

These results were obtained from the SMA thermo-mechanical constitutive model derived in Section 2. The yield stress for the transformation varies as the applied temperature varies. The generating force also varies as the temperature applied to the SMA varies. These results show that the SMA actuation force can be applied to morph a structure. In addition, using the proper residual stress, SMA wire can be actuated in the acceptable range of temperature that we are to apply.

5.2. Numerical simulation of SMA–composite structure: case 1

We first considered the SMA–composite structure whose schematic device is shown in Fig. 4. Both edges of the composite panel do not move toward the z direction, and the SMA wire is attached to the mid point of the panel. The attached SMA wire which is initially in the austenite phase state was fully transformed into the fully detwinned martensite state at room temperature 301 K. The recovery force of host structure generates the residual stress in the SMA wire. And the recovery force is large enough to make SMA wire be fully transformed to the detwinned martensite phase.

For numerical simulation of the behavior of this device, we used the first order shear deformable composite plate theory with large deflection (von Karman plate theory) for the host structure. First, we simulated the behavior of the SMA wire and panel for two cases of layers (16-ply and 24-ply plates). Next, the case of two different SMA wire lengths was simulated.

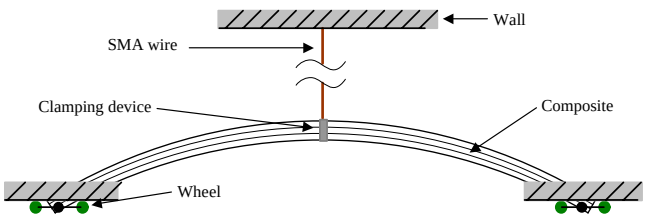

Fig. 4. Schematic of actuator device for repeated application: case 1.

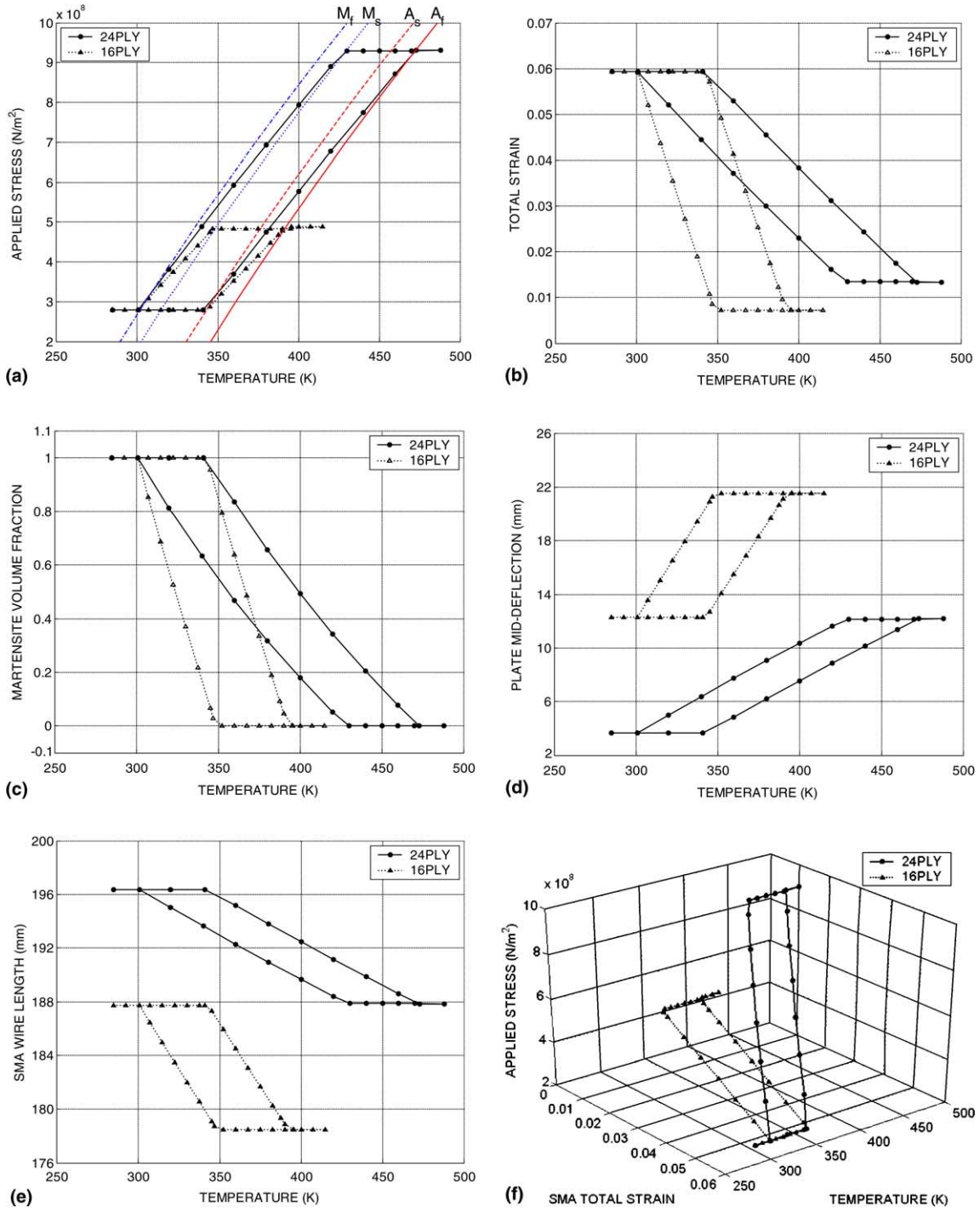

Fig. 5. (a) Stress–temperature curve for the two different layers, (b) total strain–temperature curve for the two different layers, (c) martensite volume fraction–temperature curve for the two different layers, (d) plate center deflection–temperature curve for the two different layers, (e) SMA length–temperature curve for the two different layers, (f) stress–total strain–temperature curve for the two different layers.

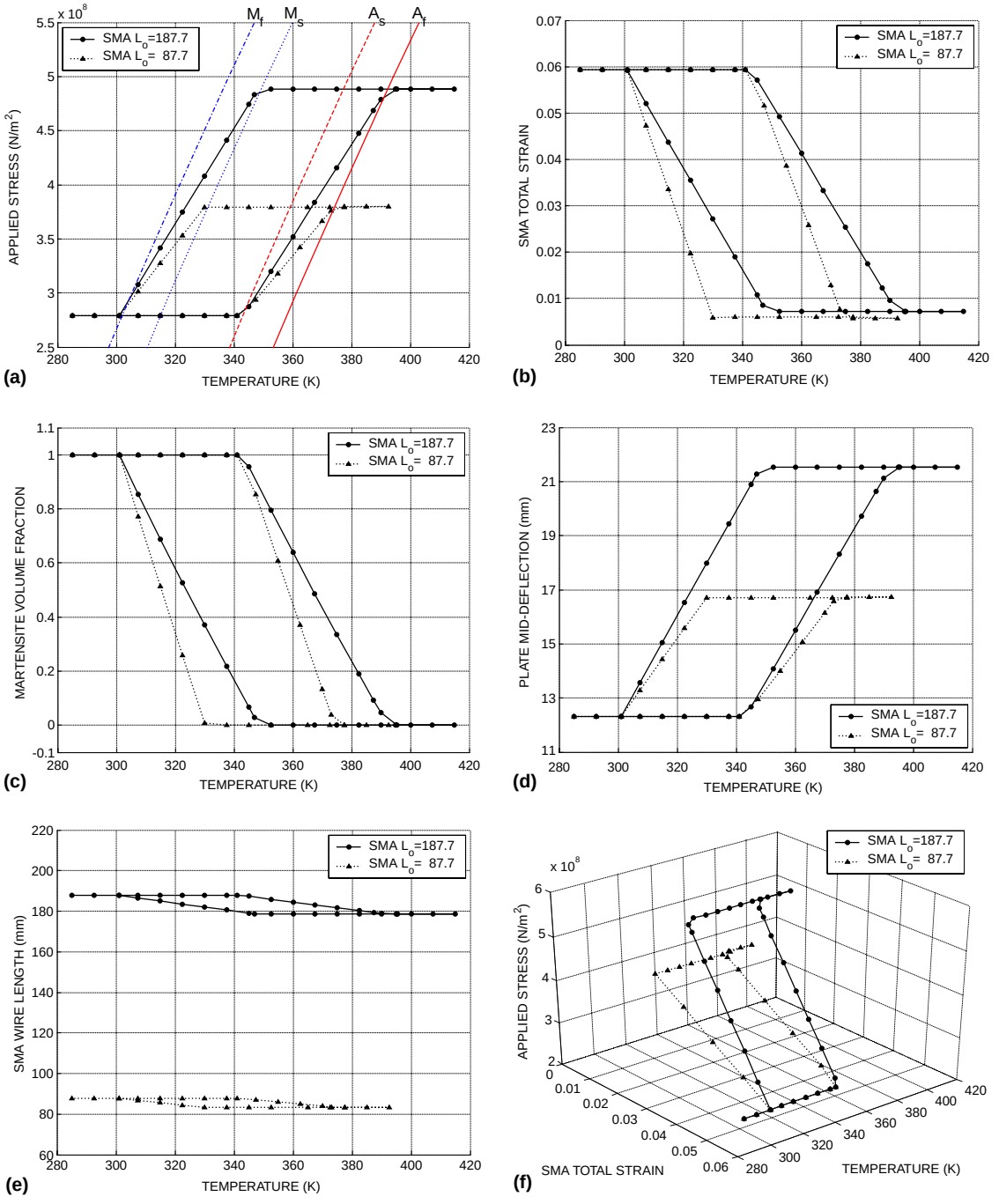

Fig. 6. (a) Stress–temperature curve for the two different wire lengths of SMA, (b) total strain–temperature curve for the two different wire lengths of SMA, (c) martensite volume fraction–temperature curve for the two different wire lengths of SMA, (d) plate deflection–temperature curve for the two different wire lengths of SMA, (e) SMA length–temperature curve for the two different wire lengths of SMA, (f) stress–total strain–temperature curve for the two different wire lengths of SMA.

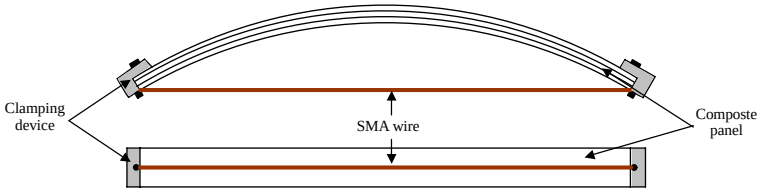

Fig. 7. Schematic of actuator device for repeated application: case 2.

In the present study, two different quasi-isotropic lay-up configurations $[0/45/90/-45]_{2s}$ and $[0/45/90/-45]_{3s}$ were considered. The numerical simulations were performed with various numbers of layers and wire length of SMA. The results are depicted in Fig. 5 and Fig. 6, respectively. The number of layers is a simulation parameter in Fig. 5.

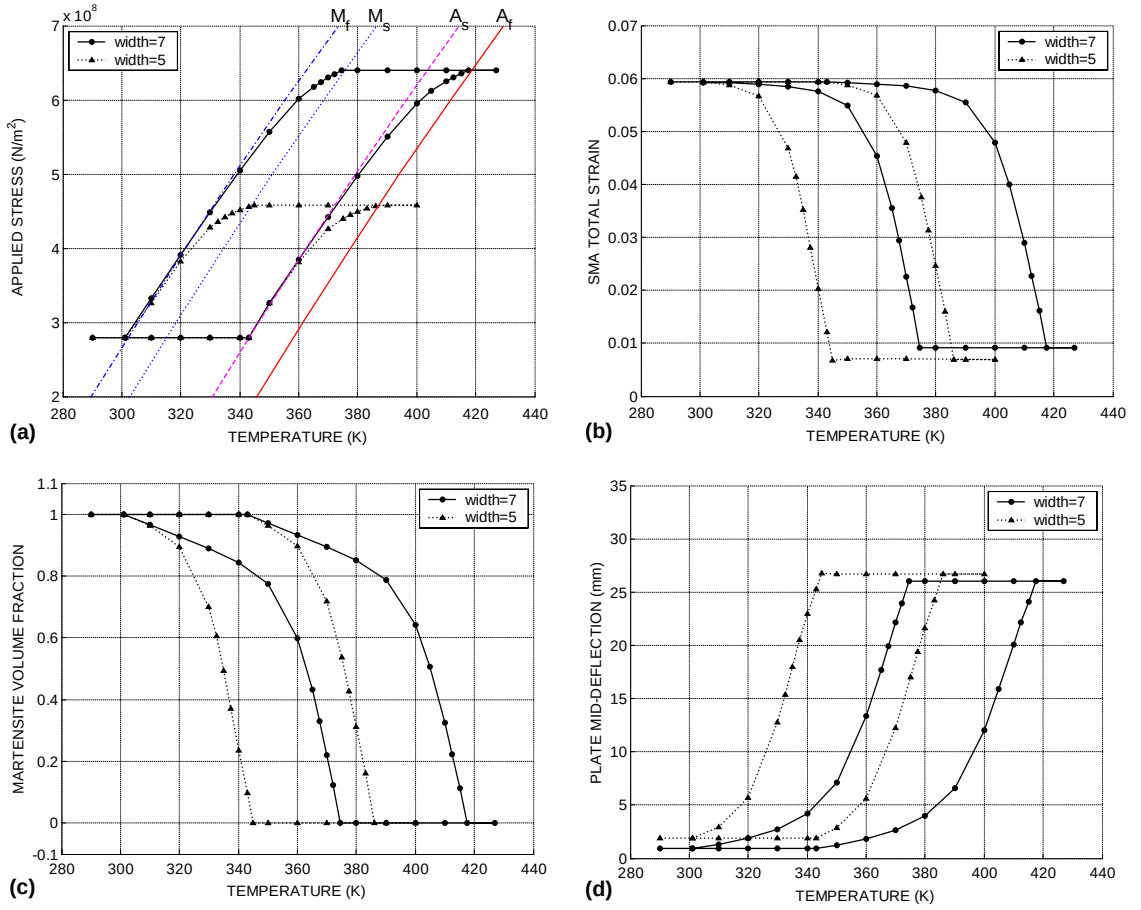

Fig. 8. (a) Stress–temperature curve for case 2, (b) total strain–temperature curve for case 2, (c) martensite volume fraction–temperature curve for case 2, (d) plate center deflection–temperature curve for case 2, (e) SMA length–temperature curve for case 2, (f) stress–total strain–temperature curve for case 2, (g) force–deflection–temperature curve for case 2, (h) force–deflection curve for case 2, (i) SMA–composite structure behavior in cooling process for case 2 (Width 7 mm).

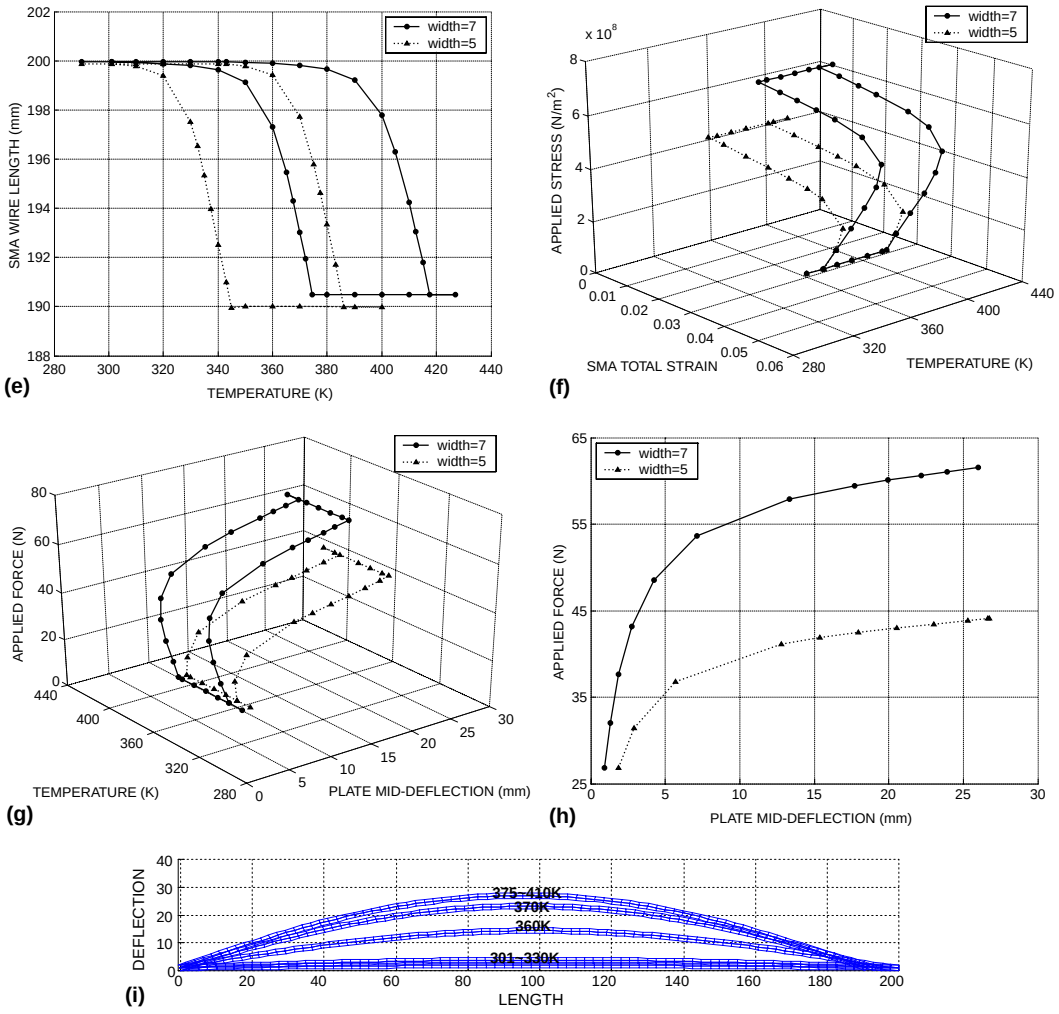

Fig. 8 (*continued*)

As shown in Fig. 5(a), for example, in the case of the actuator with the 24-ply host structure, in heating process, the actuator is not deformed until the temperature of SMA reaches austenite start temperature with the residual stress. Then the actuator is deformed linearly while the temperature of SMA changes austenite start to austenite finish temperature. Above austenite finish temperature with the residual stress, the actuator is in the fully deformed state and is not deformed by heating any more. In cooling process after fully deformed by heating, the actuator is not deformed in backward direction until the temperature of SMA reaches martensite start temperature with the residual stress. Then the actuator is deformed linearly and reversely while the temperature of SMA changes from martensite start to martensite finish temperature. Below martensite finish temperature with the residual stress, the actuator returns to its initial shape. As shown in Fig. 5(d), the initial deflection of the structure with residual stress is larger in the thin laminates than the thick laminates because the thick one is stiffer than the thin one. With fewer layers (number of layer = 16), internal variables, except the increment of stress, change rapidly. For stiffer host structures, the SMA–composite structure is actuated under a relatively high temperature and large stresses. The

deformation behavior of the current SMA actuation device for three parameters is shown in Fig. 5(f). As the number of layer becomes larger, the larger actuating range of stress and temperature is required.

The wire length of SMA is a simulation parameter in Fig. 6. The length of SMA wires are 87.7 mm and 187.7 mm respectively (i.e., the lengths between edge of the panel and ceiling are 100 mm and 200 mm respectively). The deformation rate remains almost unchanged. As shown in Fig. 6(a) and (e), the stress that causes the maximum deformation is proportional to the length of SMA wire. In addition, a larger range of temperature is required to actuate longer SMA wires. Fig. 6(f) shows the stress–total strain–temperature relationship three dimensionally. As the SMA wire length gets longer, the relatively larger actuating range of stress and temperature is required.

Considering the parametric studies on the number of the layers of composite plates and the length of a SMA wire, the effect of the host structure stiffness on the morphing of SMA–composite structure is much larger than that of the length of SMA wire.

5.3. Numerical simulation of SMA–composite structure: case 2

Second, we consider a SMA–composite device whose schematic is shown in Fig. 7. An SMA wire is attached to both edges of the composite panel. Similar to the preceding device (Fig. 4), the SMA wire has been fully transformed at the room temperature, 301 K. For numerical simulation of this device, we use the large deformable beam theory for host structure. The host structure of actuators can be analyzed by only two-dimensional plate model but we wanted to show various types of finite elements can be employed in host structure modeling. In this reason, we use the plate model for the first case and the 2D beam model for the second case. To avoid the in-plane shear locking phenomena in the plane bending deformation of beam model, the nine-node element is used. The lay-up configurations of the beam are given as $[0/45/90/-45]_{2s}$. While most of the previous researches have reported the linear behaviors only, in the present study, the characteristics of nonlinear behavior of SMA actuator-host structure assembly are considered and the nonlinear behavior is shown significant in this device.

The simulation results of the device given in Fig. 7 are shown in Fig. 8. The stress–temperature curve is almost linear, but the internal variables except stresses rapidly changes in the temperature range 320–343 K for the 5 mm-width case and in the temperature range 340–373 K for the 7 mm-width in 16-ply composite beam during cooling process. This rapid change coincides with the fact that structures deform abruptly at the critical load. Fig. 8(f) shows the behavior of the SMA wire, and Fig. 8(g) and (h) depict the temperature–force–deflection relationship and the force–deflection behavior of the host structure, respectively. The deformed shapes at the various temperatures of SMA wire in cooling process are plotted for the 16-ply composite beam in Fig. 8(i).

6. Conclusion

Until now, research for SMA was limited to the study of the thermo-mechanical behavior of SMA materials and to the one-way actuator application. However, one-way shape memory effect cannot be properly applied to repeated actuation because structures cannot recover their original shape after the SMA wire is cooled to room temperature. Besides, commonly the martensite finish temperature is too low to utilize the two-way SMA effect without the residual stresses in the SMA actuator.

Thus, two-way SMA effect under residual stress was considered in the present study. The effect of residual stress of the SMA–composite system makes the host structure returns to its original shape after cooling down to the desired temperature (for example, room temperature). The stiffness of host structure and the length of the SMA wire are two most important parameters in the design morphing structures with an SMA wire. The geometric nonlinearity of the host structure was considered because the SMA wire generates large

actuation strain, which causes the large deflection of the host structure. The deformation analysis of the SMA wire through the constitutive equation of SMA and the FE analysis of the host structures were combined to predict the behavior of a smart structure with an SMA wire. Two simple devices using the two-way shape memory effect were proposed and they were useful as actuation devices, as confirmed by numerical simulations. To validate the performance of the proposed devices, experimental study is under progress. The present actuation devices using the two-way shape effect can be applied to various structures requiring shape-morphing.

Acknowledgment

This work was supported by Smart UAV Development Center (SUDC) of the 21st Century Frontier Research Program funded by the Ministry of Science and Technology, Republic of Korea.

References

Abeyaratne, R., Kim, S.J., 1997. Cyclic effects in shape-memory alloys: a one-dimensional continuum model. Int. J. Solids Struct. 34, 3273–3289.

Abeyaratne, R., Kim, S.J., Knowles, J.K., 1993. One-dimensional continuum model for shape memory alloys. Int. J. Solids Struct. 31, 2229–2249.

Araujo, C.J., Morin, M., Guenin, G., 1999. Electro-thermomechanical behaviour of a Ti–45.0Ni–5.0Cu (at.%) alloy during shape memory cycling. Mater. Sci. Eng. A 273–275, 305–309.

Birman, V., 1997. Review of mechanics of shape memory alloy structures. Appl. Mech. Rev. 50 (11), 629–649.

Bo, Z., Lagoudas, D.C., 1999. Thermomechanical modeling of polycrystalline SMAs under cyclic loading, Part III: evolution of plastic strains and two-way shape memory effect. Int. J. Eng. Sci. 37, 1175–1203.

Boyd, J.G., Lagoudas, D.C., 1996. A thermodynamic constitutive model for the shape memory alloy materials Part I, the monolithic shape memory alloy. Int. J. Plasticity 12, 805–842.

Brinson, L.C., 1993. One-dimensional constitutive behavior of shape memory alloys: thermomechanical derivation with non-constant material functions and redefined martensite internal variable. J. Intell. Mater. Syst. Struct. 4, 229–242.

Brinson, L.C., Lammering, R., 1993. Finite element analysis of the behavior of shape memory alloys and their application. Int. J. Solids Struct. 30, 3261–3280.

Lagoudas, D.C., Bo, Z., Qidwai, M.A., 1996. A unified thermodynamic constitutive model for SMA and finite element analysis of active metal matrix composite. Mech. Compos. Mater. Struct. 3, 153–179.

Liang, C., Rogers, C.A., 1990. One-Dimensional thermomechanical constitutive relations for shape memory materials. J. Intell. Mater. Syst. Struct. 1, 207–234.

Liang, C., Rogers, C.A., 1992. Design of shape memory alloy actuators. J. Mech. Des. 114, 223–230.

Lubliner, J., 1990. Plasticity Theory. Macmillan Publishing Company, New York.

Ortin, J., Planes, A., 1989. Thermodynamics of thermoelastic martensitic transformations. Acta Metall. 37 (5), 1433–1441.

Qidwai, M.A., Lagoudas, D.C., 2000. Numerical implementation of a shape memory thermomechanical constitutive model using return mapping algorithms. Int. J. Numer. Meth. Eng. 47, 123–1168.

Raniecki, B., Lexcellent, C., 1994. R-Models of pseudoelasticity and their specification L for shape memory solids. Eur. J. Mech., A 13 (1), 21.

Šak, A.J., Cartmell, M.P., Ostachowicz, W.M., Wiercigroch, M., 2003. One dimensional SMA models for use with reinforced composite structures. Smart Mater. Struct. 12, 338–346.

Simo, J.C., Hughes, T.J.R., 1998. Computational Inelasticity. Springer-Verlag, New York Inc.

Sun, Q.P., Hwang, K.C., 1993a. Micromechanics modelling for the constitutive behavior of polycrystalline shape memory alloys-I. derivation of general relations. J. Mech. Phys. Solids 41 (1), 1–17.

Sun, Q.P., Hwang, K.C., 1993b. Micromechanics modelling for the constitutive behavior of polycrystalline shape memory alloys-II. study of the individual phenomena. J. Mech. Phys. Solids 41 (1), 19–33.

Tanaka, K., Kobayashi, S., Sato, Y., 1986. Thermomechanics of transformation pseudo-elasticity and shape memory effect in alloys. Int. J. Plasticity 2, 59–72.

Truesdell, C., Noll, W., 1965. The Non-linear Field Theories of Mechanics. Springer-Verlag, Berlin.

Zienkiewicz, O.C., Taylor, R.L., 2000. Finite Element Method. Butterworth–Heinemann.